Journal of Applied Polymer Science

Noncovalent assembly of carbon nanofiber-layered double hydroxide as a reinforcing hybrid filler in thermoplastic polyurethane-nitrile butadiene rubber blends

S. Roy,[1] S. K. Srivastava,[1] V. Mittal[2]

[1]Department of Chemistry, Indian Institute of Technology, Kharagpur 721302, India

[2]Department of Chemical Engineering, Petroleum Institute, Abu Dhabi, United Arab Emirates

Correspondence to: S. K. Srivastava (E-mail: sunit@chem.iitkgp.ernet.in)

ABSTRACT: A new synthetic route was applied to develop carbon nanofiber (CNF)–layered double hydroxide (LDH) hybrid through a noncovalent assembly using sodium dodecyl sulfate as bridging linker between magnesium–aluminum LDH and CNF and then characterized. Furthermore, this hybrid was used as nanofiller in thermoplastic polyurethane–acrylonitrile butadiene rubber (TN; 1:1 w/w) blend. Mechanical measurements showed that the 0.50 wt % hybrid loaded TN blend exhibited the maximum improvements in the elongation at break, tensile strength, and storage modulus of 1.51 times and 167 and 261% (25 °C), respectively. Differential scanning calorimetric analysis and thermogravimetric analysis showed maximum improvements in the melting temperature (5 °C), crystallization temperature (17 °C), and thermal stability (14 °C) in the 0.50 wt % surfactant modified carbon nanofiber–LDH loaded blend compared to the neat blend. Such enhancement in the properties of the TN nanocomposites could be attributed to the homogeneous dispersion, strong filler–blend interfacial interaction, and synergistic effect. © 2016 Wiley Periodicals, Inc. J. Appl. Polym. Sci. **2016**, *133*, 43470.

KEYWORDS: blends; composites; mechanical properties; micelles; thermal properties

Received 30 September 2015; accepted 23 January 2016
DOI: 10.1002/app.43470

INTRODUCTION

Recently, different forms of carbon allotropes with different structures have drawn much attention from researchers because of their unique structures, functionalities and interesting applications.[1–6] One-dimensional porous carbon nanofibers (CNFs) are one such material because of their high aspect ratio, large surface area, excellent thermal and electrical conductivities, and high temperature resistance; these make them capable materials for biosensors, electrochemical substances, Li-ion batteries, energy storage devices, and nanofillers for polymer nanocomposites.[6–11] Layered double hydroxide (LDH) is an anionic clay having the general formula $[M^{II}_{(1-x)}M^{III}_{x}(OH)_2]^{x+}A^{m-}_{m}.nH_2O$, where M^{II} and M^{III} are divalent and trivalent metal cations, respectively; A is an exchangeable interlayer anion; and x is the $M^{III}/(M^{II}+M^{III})$ molar ratio and generally has a value ranging from 0.2 to 0.33.[12] LDH also has potential applications in the fields of polymer nanocomposites,[12,13] catalysts,[14] drug delivery,[15] and environmental protection.[16] However, the applications of both CNFs (one-dimensional) and LDH (two-dimensional) are limited because of their tendency to agglomerate unless they are modified.[8,13] In recent years, the hybridization of CNFs with Fe_3O_4,[11] MoS_2,[9] and LDH[17–21] has overcome such problems faced by the individual counterparts. These hybrid structures have the combined merits of the individual components and have a fascinatingly wide range of applications[17–21] compared to the individual components. These CNF–LDH hybrids were prepared by the hybridization of one-dimensional CNFs and two-dimensional LDH platelets by *in situ* growing method[17] and pore precipitation of LDH on CNFs.[18–21] Furthermore, multiwalled carbon nanotube (MWCNT)–montmorillonite,[22] MWCNT–graphene,[23] MWCNT–LDH,[24] and so forth have been found to be very effective as three-dimensional nanofillers in polymer nanocomposites because of a synergistic effect.

Polymer blends are prepared by a combination of at least two polymers with properties that are different from their individual components.[11,13,25,26] They can be divided into immiscible, miscible, and compatible polymer blends. However, considerable attention has been focused on compatible polymer blends because of the attainment of balanced properties.[13,25] Furthermore, these polymer blends, having a variety of nanofillers, are

Additional Supporting Information may be found in the online version of this article.

capable of having properties of polymer blends and the merits of polymer nanocomposites.[11,13,25,26] In view of this, the blending of thermoplastic polyurethane (TPU) with acrylonitrile butadiene rubber (NBR) has experienced appreciable recognition for its applications in gaskets/coextrusion automotive gaskets, tubing pipes, protective covers, grips, and so on.[13,25,26] The choice of these individual polymers in TPU/NBR blends is guided by the merits of the individual components. TPU has an excellent mechanical strength, outstanding abrasion resistance, and a high shear strength but poor thermal stability, barrier properties, and weather and solvent resistance; this has been found to improve when NBR is blended with TPU. On the other hand, the poor tensile strength and ozone resistance of NBR can also promoted through blending with TPU. Therefore, it is worth studying the effect of the blending of these two polymers and further reinforcing them with fillers to investigate their various properties. Desai *et al.*[25] prepared TPU:NBR blends with various compositions (30:70, 50:50, and 70:30 w/w) and inferred the formation of the cocontinuous phase in TPU:NBR (50:50) blend due to its uniformly dispersed phases. Furthermore, there exist only limited works on carbon black, LDH, and silica filled nanocomposites of TPU/NBR blends.[13,25,26] However, no work has been reported to the best of our knowledge to study the change in the properties of TPU/NBR blend filled with CNF–LDH hybrids as nanofillers. We anticipated that such thermally and mechanically enhanced TN blend nanocomposites could find relatively better applications in the fields mentioned earlier. Motivated by these facts, in this present study, for the very first time, we proposed a facile and successful route for hybridizing CNFs with LDH by noncovalent assembly using sodium dodecyl sulfate (SDS) as a linker between them. Subsequently, the formation and morphology of the hybrid nanostructure was characterized through X-ray diffraction (XRD) analysis, Fourier transform infrared (FTIR), field emission scanning electron microscopy (FESEM), and transmission electron microscopy (TEM). Furthermore, the thus obtained hybrid was used as nanofiller for the first time in the polymer matrix, that is, the TPU/NBR (referred as TN) blend. These TN blend nanocomposites are likely to exhibit enhanced mechanical and thermal properties in the presence of this hybrid nanofiller because of synergistic effect.

EXPERIMENTAL

Materials

The thermoplastic elastomer, TPU (Desmopan-9385, Bayer, Germany), was a polyether type with melt flow rate of 4 cm^3/10 min and a density of 1.12 g/cm^3. The nitrile butadiene elastomer, NBR (Krynac 2865F), was kindly supplied by Lanxess (Germany). CNF (carbon > 99.9%, outside Diameter × Length = 100 nm × 20–200 μm) was purchased from Sigma-Aldrich. SDS (SRL Pvt., Mumbai, India), $Mg(NO_3)_2{\cdot}6H_2O$, and $Al(NO_3)_3{\cdot}9H_2O$ (E. Merck, India); NaOH (S. D. Fine Chemicals, Boisar); the cross-linking agent, dicumyl peroxide i.e. DCP (DiCUP-98, Hercules), and dry tetrahydrofuran (THF) were used as received.

Preparation of LDH

Magnesium LDH was prepared through a standard coprecipitation method followed by thermal crystallization.[13] In this procedure, $Mg(NO_3)_2{\cdot}6H_2O$ (19.65 g/0.075 mol) and $Al(NO_3)_3{\cdot}9H_2O$ (9.25 g/0.025 mol) were dissolved in 100 mL of water, subsequently added dropwise to 100 mL of an aqueous solution of NaOH (8 g/0.2 mol), placed inside a round-bottomed flask, and subjected to vigorous stirring, with the pH of the solution maintained at 10 ± 0.1 with the help of a 1 *M* NaOH solution. The white slurry so formed was left to age at 70–75 °C for 15 h followed by its filtration, washing, and drying at room temperature for 24 h.

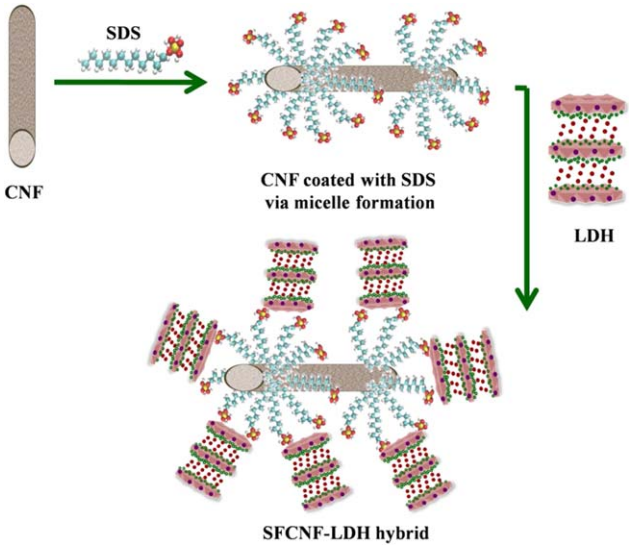

Scheme 1. Formation of SFCNF–LDH through the noncovalent assembly. [Color figure can be viewed in the online issue, which is available at wileyonlinelibrary.com.]

Preparation of the Surfactant Modified Carbon Nanofiber (SFCNF)

The modification of the pristine carbon nanofiber (PCNF) was carried out by a simple solution mixing method through micelle formation.[27] In this method, 1 mg/mL PCNF was dispersed into an aqueous solution of 1% SDS; this was greater than the critical micellar concentration.[27,28] This was followed by the centrifugation of this solution. The product so obtained was dried for 24 h at room temperature and is referred to as SFCNF.

Preparation of the SFCNF–LDH Hybrid

An aqueous suspension of 0.1 g of LDH was added to a round-bottomed flask consisting of 0.2 g of SFCNF placed in 50 mL of deionized water. Subsequently, the entire solution was vigorously stirred at 70 °C for 15 h followed by refluxing at 100 °C for 6 h. Finally, the product (referred to as the SFCNF–LDH hybrid) was filtered and dried under vacuum at 60 °C for 24 h. Scheme 1 represents the formation of the SFCNF–LDH hybrid through the noncovalent assembly of CNF and LDH using SDS.

Fabrication of the TN Nanocomposites Containing the SFCNF–LDH Hybrid

The solution intercalation method was adopted to fabricate the SFCNF–LDH hybrid filled TN nanocomposites. Accordingly, 0.25 wt % SFCNF–LDH hybrid was sonicated in 15 mL of dry THF for 30 min; this was followed by its slow addition to a

solution of 5 g of TPU and NBR (50:50 wt %) in 50 mL of THF. Thereafter, stirring was extended for another 3 h to ensure good dispersion of SFCNF–LDH in the polymer matrix. Finally, 2-phr DCP with respect to NBR was added to the solution to cure NBR, and continued stirring for another 30 min, then cast it at room temperature in a Teflon petri dish, and left it to evaporate the THF. The dried film obtained in this manner was roll-milled at room temperature and subjected to compression molding at 165 °C for 6 min to obtain the sheets of TN nanocomposites. The other nanocomposites, having 0, 0.50, 0.75, and 1 wt % SFCNF–LDH hybrid filler, were also prepared in this manner under similar conditions.

Characterization

Room-temperature wide-angle X-ray diffraction (WAXD) analysis was carried out in a PaNalytical instrument (PW3040/60, X'Pert Pro) with Cu Kα radiation ($\lambda = 0.1542$ nm) in the range of diffraction angles of $2\theta = 5$–70° at a scanning rate of 3 °/min. The average crystallite size (L_{hkl}) of the samples was calculated with the Scherrer equation[27]:

$$L_{hkl} = \frac{k\lambda}{\beta \cos\theta}$$

where k is a constant (0.9), λ is the wavelength of the radiation ($\lambda = 0.15418$ nm), β is the full width of the hkl peak at half-maximum intensity, and θ is the Bragg angle. FTIR spectra of the samples were recorded on a PerkinElmer RXI FTIR spectrometer (wave-number range = 400–4000 cm^{-1}). FESEM and high-resolution transmission electron microscopy (HRTEM) images of the hybrid filler and its corresponding TN blend composites were taken on a Carl Zeiss Supra 40 (accelerating voltage = 20 kV) and JEOL 2100 TEM instrument (acceleration voltage = 200 keV). When hybrid powder was used, the sample was sonicated in THF solution and was then drop-cast onto the copper grid, whereas, in its TN blend, the films were subjected to ultramicrotomy with a Leica ultracut UCT. After this, the cryosections 50–70 nm in thickness were obtained with freshly sharpened glass knives with cutting edges of 45° at −50 °C (sample) and −60 °C. The cryosections were collected individually on a 300-mesh copper grid. Dynamic mechanical analysis (DMA) was carried with the help of dynamic mechanical analyzer (DMA Q800, TA Instruments, Lukens Drive, Newcastle, DE) on 10 × 6 × 1.5 mm films at a frequency 1 Hz and a heating rate of 3 °C/min over a temperature range of −80 to 60 °C. The tensile analysis was performed according to the ASTM D 412-98 standard method with a Tinius Olsen h10KS universal testing machine at 25 °C with a crosshead speed of 200 mm/min. Nine dumbbell-shaped specimens (total length of the dumbbell = 70 mm) with a working length of 30 mm, a width of 4 mm, and a thickness of 0.53–0.56 mm were punched from the respective polymer films. Thermal stability measurements were analyzed in range 50–600 °C at a heating rate of 10 °C/min under nitrogen atmosphere in a Discovery thermogravimetric analyzer (TA Instruments). Differential scanning calorimetry (DSC) data of these samples were determined by means of a 204 F1 Phoenix DSC instrument from Netzsch in the temperature range −65 to 250 °C (scan rate = 10 °C/min) under a nitrogen atmosphere with a heating–cooling–heating cycle.

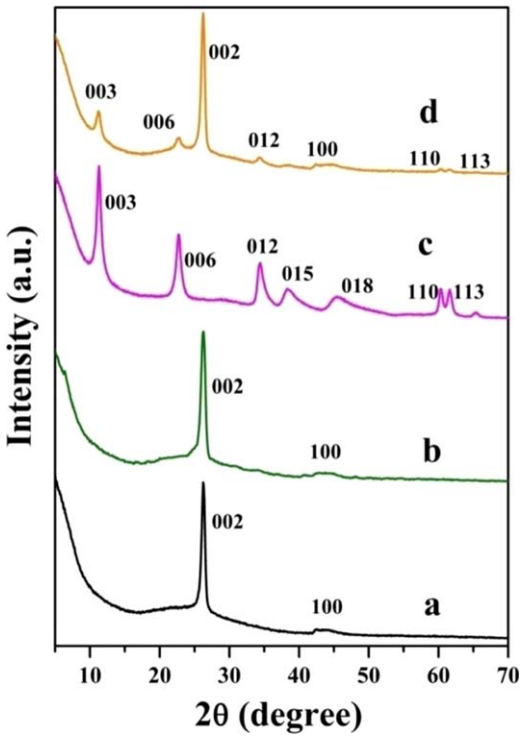

Figure 1. XRD patterns of (a) PCNF, (b) SFCNF, (c) LDH, and (d) SFCNF–LDH. [Color figure can be viewed in the online issue, which is available at wileyonlinelibrary.com.]

RESULTS AND DISCUSSION

Establishment for the formation and Nanostructure of the SFCNF–LDH Hybrid

XRD of the PCNF, SFCNF, LDH, and SFCNF–LDH hybrid are displayed in Figure 1. PCNF exhibited a sharp peak at $2\theta \sim 26.3°$ corresponding to the graphitic crystallite (002) plane ($d_{002} = 0.33$ nm).[6] In addition, another peak of moderate intensity also appeared in the diffractogram of PCNF at $2\theta \sim 43°$ corresponding to the 100 plane.[6] Interestingly, XRD of SFCNF remained almost identical to that of PCNF. LDH showed the presence of characteristic peaks at 2θs of 11.3, 22.6, 34.4, 38.3, 45.6, 60.1, and 61.6° corresponding to the (003), (006), (012), (015), (018), (110), and (113) planes, respectively.[22] The presence of the characteristic peaks of LDH and SFCNF was evident from the diffractogram of the SFCNF–LDH hybrid, although the intensity of the peaks corresponding to LDH decreased significantly in the hybrid, in all probability because of the electrostatic interaction between SFCNF and LDH in the hybrid. Interestingly, the basal spacing ($d_{003} = 0.76$ nm) in the SFCNF–LDH nanohybrids was consistent with the carbonate-intercalated LDH materials.[22] In addition, the Scherrer equation[22] was used to calculate the crystallite sizes of the PCNF, SFCNF, and SFCNF–LDH corresponding (002) planes and the respective data of the full width at half-maximum (FWHM) and crystallite size are recorded in Table I. The values from of PCNF, SFCNF, and SFCNF–LDH were found to be 15.02, 14.0,

Table I. Structural Data for the PCNF, SFCNF, and SFCNF–LDH Hybrid

Sample	FWHM (°)	Crystallite size (nm)
PCNF (002 plane)	0.54	15.02
SFCNF (002 plane)	0.58	14.0
SFCNF–LDH hybrid (002 plane)	0.69	11.75

and 11.75 nm, respectively. The observed reduction in the crystallite size of SFCNF compared to PCNF could be ascribed to the inhibiting action of SDS to form larger crystallites.[29] However, the significant reduction of crystallite size in the SFCNF–LDH hybrid compared to SFCNF was in all probability because of the confinement of SFCNF in LDH.[22,29]

The FTIR spectra of the PCNF, SFCNF, LDH, and SFCNF–LDH hybrid are displayed in Figure 2. The appearance of peaks in PCNF at about 3378, 1641,1569, and 1380 cm^{-1} were ascribed to the —OH, C=C, CH_2 bending mode, and C—O bonds, respectively.[7] The FTIR spectrum of SFCNF showed the presence of peaks at 3327 cm^{-1} (—OH stretching vibrations), 2926 cm^{-1} (CH_2 stretching mode), 1637 cm^{-1} (C=C bond vibrations), 1564 cm^{-1}(CH_2 bending mode), 1206 cm^{-1} (skeletal vibrations of the bridge S—O stretch), and 1058 cm^{-1} (C—C band stretching); these confirmed the successful coating of SDS on PCNF.[30] In case of LDH, a broad peak at about 3510 cm^{-1} appeared because of the stretching vibrations of hydroxyl groups

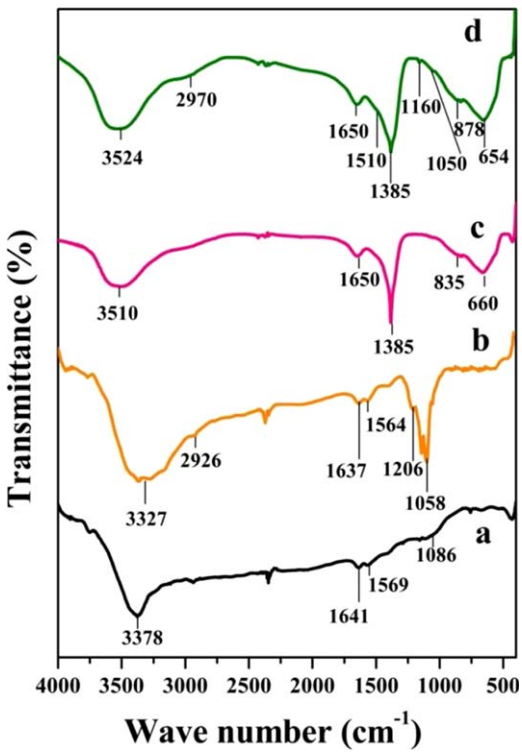

Figure 2. FTIR spectra of (a) PCNF, (b) SFCNF, (c) LDH, and (d) SFCNF–LDH. [Color figure can be viewed in the online issue, which is available at wileyonlinelibrary.com.]

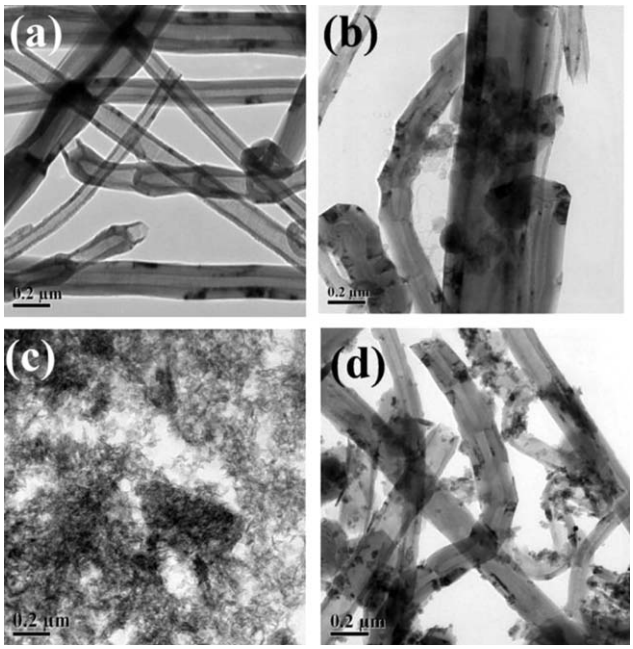

Figure 3. HRTEM images of (a) PCNF, (b) SFCNF, (c) LDH, and (d) SFCNF–LDH.

of the inorganic layers and the deformation mode of interlayer water.[31] Other additional peaks also appeared in the FTIR spectrum of LDH at 1650 cm^{-1} (deformation mode of interlayer water molecules), 1385 cm^{-1} (vibration mode of CO_3^{2-} anion), and 835 and 660 cm^{-1} (metal–oxygen stretching and bending modes).[31] The FTIR spectrum of the as-prepared SFCNF–LDH nanohybrid showed shifting of peaks corresponding to —OH stretching vibrations (3524 cm^{-1}), CH_2 stretching (2970 cm^{-1}) and bending (1510 cm^{-1}) modes, skeletal vibrations of bridge S—O stretching (1160 cm^{-1}), C—C bond stretching (1050 cm^{-1}), and metal–oxygen stretching (878 cm^{-1}) and bending (654 cm^{-1}) modes[31] compared to those of the individual SFCNF and LDH. Such observations suggested the presence of interfacial electrostatic interactions between the negatively charged sulfonate head groups (—SO_3^-) of SFCNF and the positively charged layers of LDH. Furthermore, it was noted that the peaks appearing at 1650 cm^{-1} (deformation mode of the interlayer water molecules of LDH) and 1385 cm^{-1} (vibration mode of CO_3^{2-} anion of LDH) remained unaltered; this ruled out the possibility of interaction between SFCNF and the interlayer molecules of LDH.

The morphologies of PCNF, SFCNF, LDH, and SFCNF–LDH were investigated by FESEM and are displayed in Figure S1 (Supporting Information), whereas the corresponding HRTEM images are displayed in Figure 3. It was distinctly clear that the PCNFs existed as tangled hollow cylinders,[10] with diameters ranging from about 78 to 130 nm. In the case of SFCNF, the SDS coating on the tubular surface of PCNF was clearly visible with its increased diameter in the range of about 97 to 152 nm. LDH showed a typical aggregated morphology.[32] Furthermore, the HRTEM image of the SFCNF–LDH hybrid indicated that platelike LDH was attached to the sidewalls of SFCNF because of the high affinity of the LDH platelets toward SFCNF.

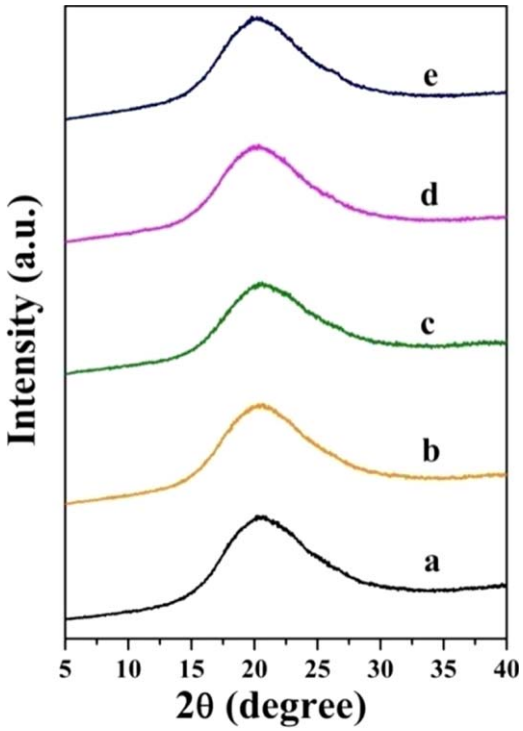

Figure 4. WAXD patterns of the (a) neat TN and its nanocomposites containing (b) 0.25, (c) 0.50, (d) 0.75, and (e) 1 wt % SFCNF–LDH hybrid. [Color figure can be viewed in the online issue, which is available at wileyonlinelibrary.com.]

Nanostructure of the TN Blend

In earlier studies, the phase morphology of the TPU:NBR blend with various ratios of TPU:NBR (30:70, 50:50, and 70:30 w/w) was investigated.[13,25] The cocontinuous phase of both components was evident in the TPU:NBR (50:50) blend from those studies. They also concluded that the components ran through one another to form an interpenetrating network; which was completely different from the results obtained from the 30:70 and 70:30 TPU:NBR blend. In last two cases, phase-separated morphology was observed. Therefore, the nanostructure of the 50:50 TN blends in the presence of SFCNF–LDH was investigated in this study.

WAXD patterns of TN and its nanocomposite containing 0.25, 0.50, 0.75, and 1 wt % SFCNF–LDH hybrid are shown in Figure 4.

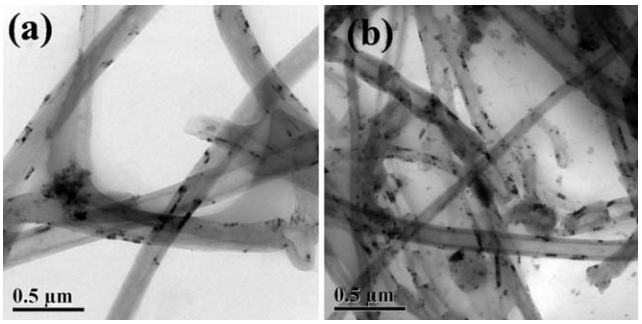

Figure 5. HRTEM images of TN nanocomposites containing (a) 0.50 and (b) 1 wt % SFCNF–LDH hybrid.

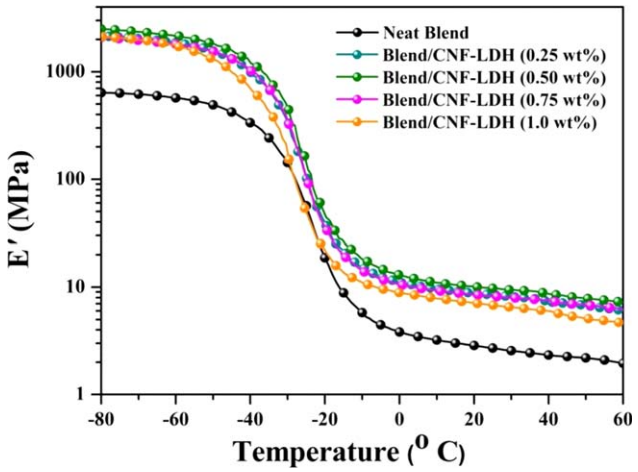

Figure 6. E′ values of the neat TN and its nanocomposites containing 0.25, 0.50, 0.75, and 1 wt % SFCNF–LDH hybrid. [Color figure can be viewed in the online issue, which is available at wileyonlinelibrary.com.]

The TN matrix exhibited a broad peak at $2\theta \sim 20°$; this was attributed to the presence of a short-range regular ordered structure of both the hard and soft segments along with the amorphous phase of the TPU matrix[22,23] and the characteristic amorphous state of NBR.[33] In the hybrid filled TN nanocomposites, the peak position remained almost identical to the neat TN, but the absence of the (003), (006), and (002) planes of the SFCNF–LDH hybrid in the TN nanocomposites indicated the formation of partially exfoliated TN nanocomposites. The FWHM values corresponding to $2\theta \sim 20°$ of the 0, 0.25, 0.50, 0.75, and 1 wt % SFCNF–LDH hybrid filled TN were found to be 8.12, 7.40, 7.24, 7.54, and 7.66°, respectively. These data signify that the SFCNF–LDH hybrid loaded TN nanocomposites formed more ordered structures compared to the neat TN itself. This could have been due to the strong interfacial interaction between the polymer matrix and the hybrid nanofiller,[22–24] although the appearance/disappearance of diffraction peaks of the hybrid filler was not the ultimate parameter for interpreting

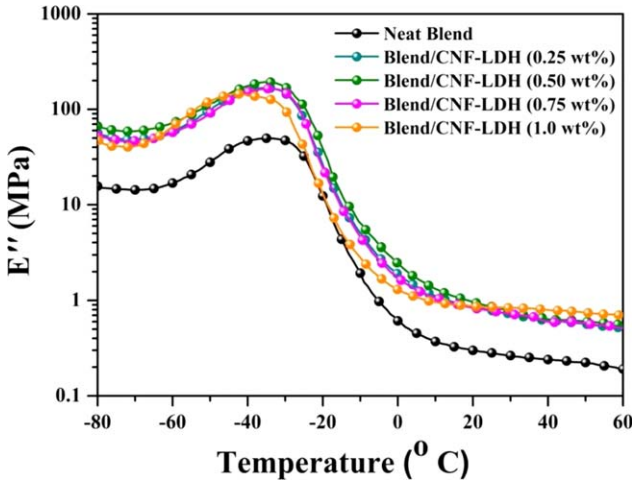

Figure 7. E″ values of the neat TN and its nanocomposites containing 0.25, 0.50, 0.75, and 1 wt % SFCNF–LDH hybrid. [Color figure can be viewed in the online issue, which is available at wileyonlinelibrary.com.]

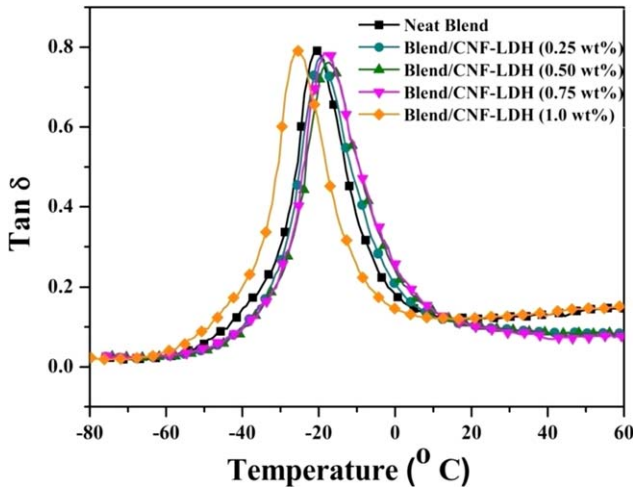

Figure 8. Temperature dependence curve of tan δ of the neat TN and its nanocomposites containing 0.25, 0.50, 0.75, and (e) 1 wt % SFCNF–LDH hybrid. [Color figure can be viewed in the online issue, which is available at wileyonlinelibrary.com.]

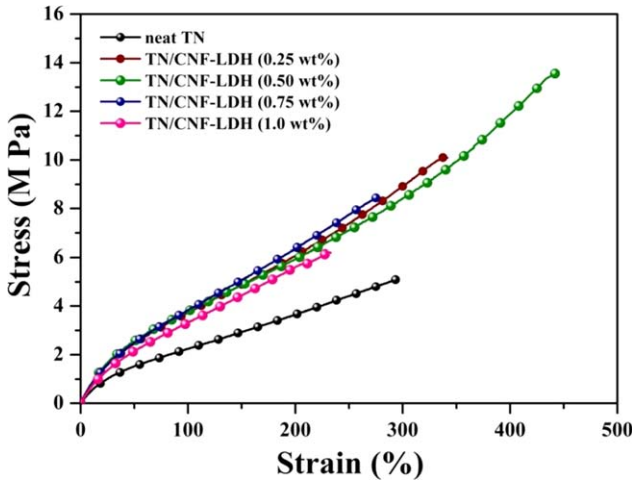

Figure 9. Representative stress–strain plots of the neat TN and its nanocomposites containing 0.25, 0.50, 0.75, and 1 wt % SFCNF–LDH hybrid. [Color figure can be viewed in the online issue, which is available at wileyonlinelibrary.com.]

the formation of intercalated or partially exfoliated nanocomposites.

Figure 5 displays the HRTEM images of TN nanocomposites containing 0.50 and 1 wt % hybrid filler. The interconnected hybrid network was spread uniformly throughout the TN matrix in the 0.50 wt % SFCNF–LDH hybrid filled TN. This was also likely to be reflected in the enhanced properties of the TN nanocomposites of SFCNF–LDH. It was also noticed that the aggregation of the hybrid filler was more dominant at 1.0 wt % filler loading in TN.

Mechanical Properties of the TN Nanocomposites

DMA provided an idea about the viscoelastic properties of the polymer. The DMA results of the neat TN and its SFCNF–LDH hybrid filled TN nanocomposites are presented in Figures 6–8, and the respective data are summarized in Table II. The storage modulus (E') describes the elastic modulus of the materials, whereas the loss modulus (E'') was associated with energy loss because of the friction generated with the polymer chain movement. Figure 6 shows that the E' values of the nanocomposites were higher than that of the neat TN; this signified the effect of the SFCNF–LDH hybrid in TN. We noted that the 0.50 wt % SFCNF–LDH hybrid filled TN matrix achieved maximum E' values up to 276% (at −60 °C) and 261% (at 25 °C). Figure 7 shows that the E'' values increased with increasing loading of the SFCNF–LDH hybrid in the TN nanocomposites compared to the neat sample. At −30 °C, the E'' values of the TN nanocomposites filled with 0.25, 0.50, 0.75, and 1 wt % hybrid were improved by 99, 254, 224, and 193%, respectively, compared to the pure TN (47.22 MPa). These results were superior to earlier reports.[13] Such enhanced E' and E'' values suggests that the hybrid filler strongly influenced the elastic properties and interacted effectively with the polymer chains; this increased the friction between the filler and polymer because of the combined effect of the dispersion of filler and the filler–polymer interaction.[13,22,23]

The effect of the SFCNF–LDH hybrid filler on the dissipation factor (tan δ) of the neat TN and its nanocomposites as a function of the temperature is displayed in Figure 8. The tan δ maxima signified the glass-transition temperature (T_g) of the neat TN and its SFCNF–LDH filled nanocomposites. The TN nanocomposites containing 0.50 wt % SFCNF–LDH hybrid filler showed a decrease in tan δ height (0.75) compared to that in the neat TN (0.79). Such findings were attributed to the internal friction among the nanofiller–nanofiller, nanofiller–polymer matrix, and polymer matrix–matrix under some external stresses.[34] Further results show that TN nanocomposites having 0.50 wt % filler exhibited the maximum positive shift in T_g (~3 °C) compared to the neat sample because of strong polymer–filler interactions, which caused a restriction in the

Table II. E′ Values at Different Temperatures, T_g Values, and Heights of the Tan δ Value for the Pure TN and Its Composites

Sample	E' at −60 °C (MPa)	E' at 25 °C (MPa)	T_g from maxima of E'' (°C)	Tan δ
Pure TN	571	2.70	−36	0.79
TN/SFCNF-LDH (0.25 wt %)	1856	8.45	−35	0.77
TN/SFCNF-LDH (0.50 wt %)	2149	9.76	−33	0.75
TN/SFCNF-LDH (0.75 wt %)	1817	8.20	−34	0.78
TN/SFCNF-LDH (1.0 wt %)	1749	6.79	−42	0.79

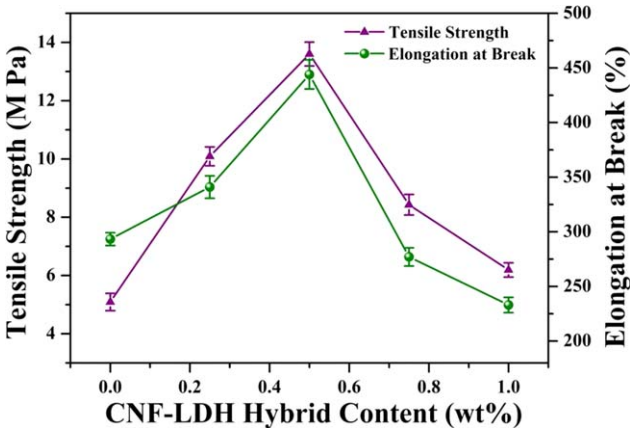

Figure 10. Variation of the tensile strength and elongation at break of the TN nanocomposites versus the SFCNF–LDH hybrid content. [Color figure can be viewed in the online issue, which is available at wileyonlinelibrary.com.]

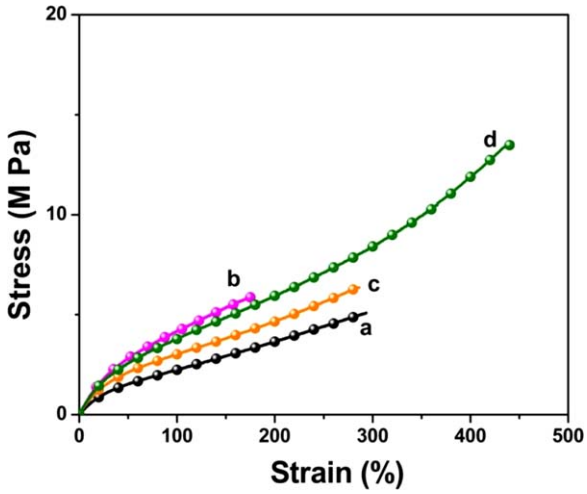

Figure 11. Representative stress–strain plots of the (a) neat TN and its nanocomposites with (b) 0.25 wt % LDH, (c) 0.25 wt % SFCNF, and (d) 0.50 wt % SFCNF–LDH hybrid. [Color figure can be viewed in the online issue, which is available at wileyonlinelibrary.com.]

mobility of the polymer chains near T_g.[35] We noted that T_g also shifted to higher values in the case of the 0.75 wt % SFCNF–LDH filler loading; this was followed by a reduction in the 1 wt % filler loaded TN blends. In all probability, this was due to the aggregation of the hybrid filler, which helped to generate void space, which acted as a defect in the matrix.[36,37] As a result, the polymer chains moved easily; this accounted for the decrease in T_g observed in the 1 wt % filler loaded TN blend. The aggregation of filler was also evident in the TEM images of 1 wt % filler loaded blend nanocomposites as discussed earlier.

Figure 9 shows the representative stress strain plot, whereas the corresponding plot of the variation of the tensile strength and elongation at break of the TN nanocomposites with respect to the SFCNF–LDH hybrid filler content is shown in Figure 10. The enhancement in the mechanical properties clearly indicated the reinforcing effect of SFCNF–LDH in the TN matrix. It was also noted that the 0.50 wt % filler loaded TN nanocomposite exhibited the maximum improvements in the tensile strength (167%) and elongation at break (1.51 times) compared to the neat TN. These findings are superior to reports in the literature.[13] Such improvements in the mechanical properties were attributed to the homogeneous dispersion of SFCNF–LDH filler

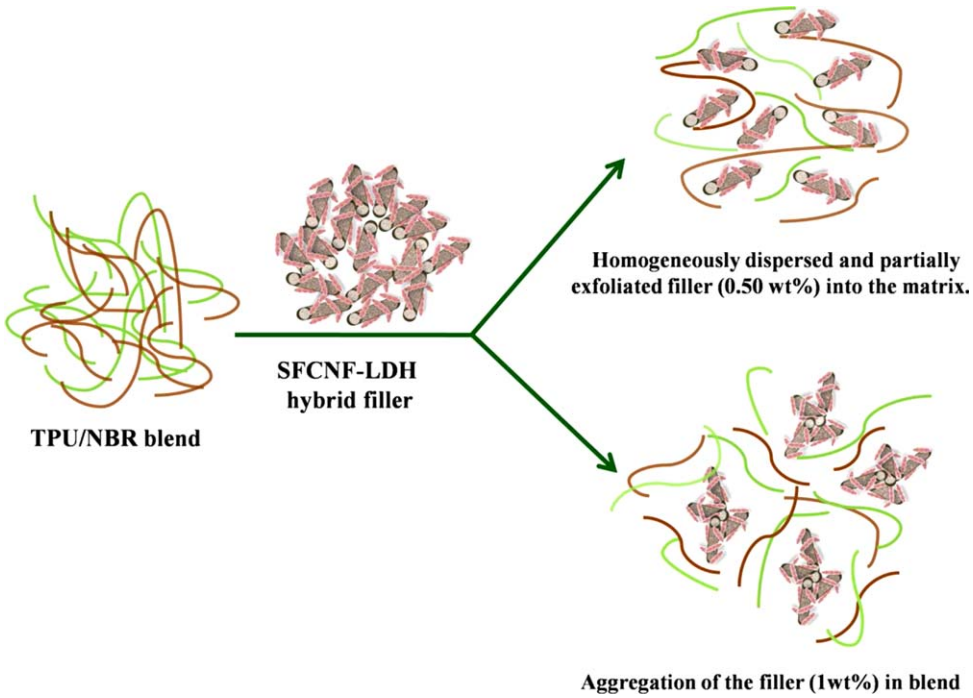

Scheme 2. TN blend without and with the filler to explain the mechanical properties. [Color figure can be viewed in the online issue, which is available at wileyonlinelibrary.com.]

Table III. TGA Data for the Neat TN and Its Nanocomposites

Sample	$T_{d(5\%)}$ (°C)	$T_{d(20\%)}$ (°C)	$T_{d(50\%)}$ (°C)	Residue at 650 °C (wt %)
Pure TN	270	344	415	1.2
TN/SFCNF–LDH (0.25 wt %)	284	342	429.7	3.2
TN/SFCNF–LDH (0.50 wt %)	286	337	429	3.9
TN/SFCNF–LDH (0.75 wt %)	285	335	426	4.1
TN/SFCNF–LDH (1.0 wt %)	280	332	424	4.5

T_5, temperature at 5% weight loss; T_{20}, temperature at 20% weight loss; T_{50}, temperature at 50% weight loss.

in the TN matrix and the strong interfacial interaction between the hybrid filler and polymer matrix.[22–24] At higher loadings, the tensile strength and elongation at break gradually decreased; this was attributed to the aggregation of the filler in the matrix. To explain the findings from the mechanical properties of the TN blend in the presence of the SFCNF–LDH hybrid filler, Scheme 2 was proposed. Furthermore, tensile measurements of the TN nanocomposites containing 0.25 wt % LDH and 0.25 wt % SFCNF were carried out, and compared the results with those of the neat TN and 0.50 wt % SFCNF–LDH hybrid loaded TN nanocomposites, shown in Figure 11. The observation showed 15.5, 24.7, and 167% improvements in the tensile strength for the TN nanocomposites having 0.25 wt % LDH, 0.25 wt % SFCNF, and 0.50 wt % SFCNF–LDH hybrid, respectively, whereas enhancements in the elongation at break were observed up to 176.7, 286.3, and 443.5% compared to the neat TN for the 0.25 wt % LDH, 0.25 wt % SFCNF, and 0.50 wt % SFCNF–LDH hybrid loaded TN nanocomposites, respectively. These findings clearly confirmed the synergistic effect of SFCNF and LDH in the mechanical properties of the TN nanocomposites. In other words, the strength of both the CNF and LDH were combined in the SFCNF–LDH hybrid; this was reflected in the enhanced mechanical strength of the blend nanocomposites in the presence of hybrid filler compared to their individual filler-loaded polymer matrixes.

Thermal Properties of the TN Nanocomposites

The thermogravimetric analysis (TGA) of the neat TN and its nanocomposites are displayed in Figure S2 (Supporting Information) and Table III. It was noted that the decomposition of TN and its nanocomposites involved three steps.[13] The first step of degradation (~230–300 °C) in the thermogram was ascribed to the rapid rapture of urethane linkages of TPU; this produced isocyanate and polyol.[13,38] The second weight loss in TGA in the range 330–480 °C was associated with the thermal degradation of isocyanate to form urea and the degradation of the butadiene segments of NBR.[38,39] The third and final weight loss in TGA above 500 °C was attributed to the decomposition of the earlier formed urea and acrylonitrile segments, which originated from NBR to yield to small amount of carbonaceous char.[13,38,39] Table III shows the thermal stability data of the neat TN and its nanocomposites corresponding to 5, 20, and 50% weight losses and the char residue at 650 °C. We inferred from the T_5 data that thermal stability of TN ($T_5 = 270$ °C) improved in the presence of the hybrid filler ($T_5 = 280$–286 °C), in all probability because of the enhanced thermal stability of the SFCNF–LDH hybrid.[40,41] Thermal data based on T_{20} suggests that the TN nanocomposites exhibited inferior thermal stability compared to the neat TN. This decrease in the thermal stability was associated with the decomposition of LDH because the CNFs were thermally stable above 800 °C.[40–42] The alkyl chains of LDH degraded; this was followed by the evaporation of the interlayer absorbed water, hydroxide, and carbonate loss on the LDH layers.[41] Such decomposition is highly advantageous in promoting the charring process and the thermal stability of the corresponding nanocomposites. This charred layer acts as a barrier by disrupting the emission of volatile degradation products throughout the composite.[13] In addition, the filler in the polymer matrix also tended to obstruct the further escape of degraded smaller molecules and, thus, hindered the degradation of the TN nanocomposites. Thermal data based on T_{50} supported this fact: the thermal stability of TN was once again enhanced in the presence of SFCNF–LDH hybrid loading. Alternatively, the possibility of strong interfacial interactions between the polymer and filler and the combined stabilizing effect of SFCNF and LDH accounting for the enhancement in the thermal stability of the TN nanocomposites also could not be ruled out.[22–24] The thermal stability was improved to a maximum degree for the 0.25 (0.50) wt % SFCNF–LDH filled TN matrix by 14 (16) and 15 (14) °C at 5 and 50% weight losses, respectively. However, the TN nanocomposite exhibited inferior thermal stability at higher filler loadings because of the aggregation of SFCNF–LDH in TN. It was observed that the char residues of the TN nanocomposites were slightly higher compared to the neat TN because of the presence of the hybrid filler.

Figures S3 and S4 (Supporting Information) display the DSC results of the neat TN and its nanocomposites; the corresponding data are summarized in Table IV. The second heating curve in Figure S3 indicates that T_g was slightly improved (5 °C) in

Table IV. T_g, T_m, and T_c of TN and Its Composites

Sample	T_g (°C)	T_m (°C)	T_c (°C)
Pure TN	−45	153	80
TN/SFCNF–LDH (0.25 wt%)	−42	156	92
TN/SFCNF–LDH (0.50 wt %)	−40	158	97
TN/SFCNF–LDH (0.75 wt %)	−43	154	95
TN/SFCNF–LDH (1.0 wt %)	−45	149	83

the presence of the hybrid filler compared to the neat TN (−45 °C) because of the restricted mobility of the polymer chains. In addition, the melting temperature (T_m) of the neat TN (153 °C) was improved to a maximum by 5 °C in the 0.50 wt % SFCNF–LDH loaded TN in all probability because of the formation of the most ordered crystallites associated with the nucleating effect of the filler.[22,23] At other filler loadings in TN, larger nucleating sites accounted for the formation of smaller crystallites with comparatively lower T_m values.[43] It was evident from the DSC studies that the crystal structure of the hybrid filler definitely affected T_m of TN because of the nucleating effect,[43] as obvious from the further DSC cooling (first) curves of the neat TN and its hybrid filled nanocomposites, as shown in Figure S4. Neat TN exhibited an exothermic peak at 80 °C [crystallization temperature (T_c)], which was attributed to the T_c of the neat blend. Figure S4 shows that T_c of the SFCNF–LDH filled TN nanocomposites increased up to 0.50 wt % filler loading (maximum 97 °C), and this improvement clearly suggested a positive heterogeneous nucleating effect of the hybrid filler, which significantly improved the intrinsic crystallization tendency of the TN matrix.[44] At higher filler loading, a decrease in T_c was attributed to the limited nucleating proficiency of the hybrid filler, and this resulted in a slower crystallization process.[45]

CONCLUSIONS

SFCNF–LDH hybrid was successfully synthesized. Subsequently, this hybrid was used to fabricate nanocomposites with TN blend, and their mechanical and thermal properties were investigated. The mechanical measurements showed the improved E' (276 and 261% at −60 and 25 °C, respectively) and tensile strength (167%) in the 0.50 wt % hybrid loaded TN nanocomposite. The maximum thermal stability was obtained (∼15 °C) at a 50% weight loss. The DSC measurements showed that incorporation of the hybrid filler in the TN matrix increased T_m (5 °C) and T_c (17 °C) of the TN matrix. The homogeneous dispersion and strong interfacial interaction between the TN matrix and filler was responsible for such enhanced properties.

ACKNOWLEDGMENTS

The authors are grateful to the Council of Scientific and Industrial Research (New Delhi, India) for its financial support. They also express their gratitude to Bayer Germany and Lanxess (Germany) for providing TPU (Desmopan-9385) and NBR (Krynac 2865F), respectively. They also express thanks to the head of the Rubber Technology Centre of the Indian Institute of Technology (Kharagpur, India) for providing compression molding and DMA.

REFERENCES

1. Wei, C.; Dai, L.; Roy, A.; Tolle, T. B. *J. Am. Chem. Soc.* **2006**, *128*, 1412.
2. Bindumadhavan, K.; Srivastava, S. K.; Mahanty, S. *Chem. Commun.* **2013**, *49*, 1823.
3. Lian, P.; Zhu, X.; Liang, S.; Li, Z.; Yang, W.; Wang, H. *Electrochim. Acta* **2010**, *55*, 3909.
4. Lu, T.; Zhang, Y.; Li, H.; Pan, L.; Li, Y.; Sun, Z. *Electrochim. Acta* **2010**, *55*, 4170.
5. Mittal, V. *Macromol. Mater. Eng.* **2014**, *299*, 906.
6. Fu, J.; Qiao, H.; Li, D.; Luo, L.; Chen, K.; Wei, Q. *Sensors* **2014**, *14*, 3543.
7. Shi, Y.; Feng, X.; Wang, H.; Lu, X. *Wear* **2008**, *264*, 934.
8. Si, Q.; Hanai, K.; Ichikawa, T.; Hirano, A.; Imanishi, N.; Yamamoto, O.; Takeda, Y. *J. Power Sources* **2011**, *196*, 6982.
9. Zhou, F.; Xin, S.; Liang, H.-W.; Song, L.-T.; Yu, S.-H. *Angew. Chem. Int. Ed.* **2014**, *53*, 11552.
10. Vellacheri, R.; Pillai, V. K.; Kurungot, S. *Nanoscale* **2012**, *4*, 890.
11. Ren, T.; Si, Y.; Yang, J.; Ding, B.; Yang, X.; Hong, F.; Yu, J. *J. Mater. Chem.* **2012**, *22*, 15919.
12. Costa, F. R.; Saphiannikova, M.; Wagenknecht, U.; Heinrich, G. *Adv. Polym. Sci.* **2008**, *210*, 101.
13. Kotal, M.; Srivastava, S. K.; Bhowmick, A. K. *Polym. Int.* **2010**, *59*, 2.
14. Wang, J.; Fan, G.; Wang, H.; Li, F. *Ind. Eng. Chem. Res.* **2011**, *50*, 13717.
15. Sels, B.; De Vos, D.; Buntinx, M.; Pierard, F.; Kirsch-De Mesmaeker, A.; Jacobs, P. *Nature* **1999**, *400*, 855.
16. Zhao, Y.; He, S.; Wei, M.; Evans, D. G.; Duan, X. *Chem. Commun.* **2010**, *46*, 3031.
17. He, F.; Hu, Z.; Liu, K.; Zhang, S.; Liu, H.; Sang, S. *J. Power Sources* **2014**, *267*, 188.
18. Meis, N. N. A. H.; Bitter, J. H.; De Jong, K. P. *Ind. Eng. Chem. Res.* **2010**, *49*, 8086.
19. Álvarez, M. G.; Frey, A. M.; Bitter, J. H.; Segarra, A. M.; De Jong, K. P.; Medina, F. *Appl. Catal. B* **2013**, *134–135*, 231.
20. Winter, F.; Koot, V.; Van Dillen, A. J.; Geus, J. W.; De Jong, K. P. *J. Catal.* **2005**, *236*, 91.
21. Winter, F.; van Dillen, A J.; De Jong, K. P. *Chem. Commun.* **2005**, 3977. DOI: 10.1039/B506173C.
22. Roy, S.; Srivastava, S. K.; Pionteck, J.; Mittal, V. *Polym. Compos.* **2014**, DOI: 10.1002/pc.23350.
23. Roy, S.; Srivastava, S. K.; Pionteck, J.; Mittal, V. *Macromol. Mater. Eng.* **2015**, *300*, 346.
24. Pradhan, B.; Srivastava, S. K. *Compos. Part A* **2014**, *56*, 290.
25. Desai, S.; Thakore, I. M.; Brennan, A.; Devi, S. *J. Macromol. Sci. Part A* **2001**, *38*, 711.
26. Tan, J. H.; Wang, X. P.; Tai, J. J.; Luo, Y. F.; Jia, D. M. *Express Polym. Lett.* **2012**, *6*, 588.
27. Zhang, S.; Wu, J.-Y.; Tse, C.-T.; Niu, *J. Sol. Energy Mater. Sol. C* **2012**, *96*, 124.
28. Tan, Q.; Zhang, K.; Gu, S.; Ren, *J. Appl. Surf. Sci.* **2009**, *255*, 7036.
29. Duan, X.; Ma, F.; Yuan, Z.; Chang, L.; Jin, X. *J. Electroanal. Chem.* **2012**, *677–680*, 90.
30. Singh, M. K.; Agarwal, A.; Gopal, R.; Swarnkar, R. K.; Kotnala, R. K. *J. Mater. Chem.* **2011**, *21*, 11074.
31. Wang, M.; Bao, W.-J.; Wang, J.; Wang, K.; Xu, J.-J.; Chen, H.-Y.; Xia, X.-H. *Sci. Rep.* **2014**, *4*, 6606.

32. Chakraborty, J.; Roychowdhury, S.; Sengupta, S.; Ghosh, S. *Mater. Sci. Eng. C* **2013**, *33*, 2168.
33. Mou, H.; Shen, F.; Shi, Q.; Liu, Y.; Wu, C.; Guo, W. *Eur. Polym. J.* **2012**, *48*, 857.
34. Ren, X.; Wang, X. Q.; Sui, G.; Zhong, W. H.; Fuqua, M. A.; Ulven, C. A. *J. Appl. Polym. Sci.* **2008**, *107*, 2837.
35. Sarwar, M. I.; Zulfiqar, S.; Ahmad, Z. *Polym. Int.* **2008**, *57*, 292.
36. Ahmad, S. H.; Tarawneh, M. A.; Yahya, S. Y.; Rasid, R. In Carbon Nanotubes—Synthesis, Characterization, Applications; Yellampalli, S., Ed.; InTech: Rijeka, Croatia, **2011**.
37. Jena, R. K.; Yue, C. Y.; Yun, K. X. *RSC Adv.* **2014**, *4*, 12448.
38. Chattopadhyay, D. K.; Webster, D. C. *Prog. Polym. Sci.* **2009**, *34*, 1068.
39. Zeid, M. M. A. *Eur. Polym. J.* **2007**, *43*, 4415.
40. Garcia-Gallastegui, A.; Iruretagoyena, D.; Mokhtar, M.; Asiri, A. M.; Basahel, S. N.; Al-Thabaiti, S. A.; Alyoubi, A. O.; Chadwick, D.; Shaffer, M. S. P. *J. Mater. Chem.* **2012**, *22*, 13932.
41. Wang, X.; Zhou, S.; Xing, W.; Yu, B.; Feng, X.; Song, L.; Yuan, H. *J. Mater. Chem. A* **2013**, *1*, 4383.
42. Wu, J.; Cai, H.; Xu, K.; Fu, Z.; Liu, X.; Chen, M.; Zhang, X. *Chem. Phys. Lett.* **2012**, *552*, 78.
43. Špírková, M.; Duszová, A.; Poręba, R.; Kredatusová, J.; Bureš, R.; Fáberová, M.; Šlouf, M. *Compos. Part B* **2014**, *67*, 434.
44. Zhao, C.-X.; Zhang, W.-D.; Sun, D.-C. *Polym. Compos.* **2009**, *30*, 649.
45. Sahoo, N. G.; Jung, Y. C.; Yoo, H. J.; Cho, J. W. *Macromol. Chem. Phys.* **2006**, *207*, 1773.